JJMIE

Volume 20, Number 1, March. 2026
ISSN 1995-6665
Pages 29– 36
https://doi.org/10.59038/jjmie/200103
Editor-in-Chief: Prof. Faris M. AL-Oqla

Jordan Journal of Mechanical and Industrial Engineering

Performance Analysis of Multibody Mechanical Systems with Imperfect Flexible Joints

Bassam J. Alshaer [a,*], Hamid M. Lankarani[b], Ahmad S. Al-Shyyab[a], Ali B. Alfreahat[a]

[a]Department of Mechanical Engineering, Jordan University of Science and Technology, Irbid 22010, Jordan

[b]Department of Mechanical Engineering, Wichita State University Wichita, KS 67260-133, USA

Received 29 Jun 2025 Accepted 5 Feb 2026

Abstract

Multibody mechanical systems consist of interconnected bodies joined by various joints. Joint imperfections, often stemming from wear, introduce clearances that result in impacts. To mitigate these effects, soft-material bushes are employed to add flexibility. This research evaluates the combined impact of joint flexibility and imperfections on system performance. A mathematical model for the dynamic equations of motion is formulated. The performance of a crank-slider mechanism with imperfect, flexible joints is examined using advanced commercial software that integrates Multibody System dynamics with the Finite Element Method. The findings indicate that while mechanisms with ideal rigid joints exhibit optimal performance, such joints are impractical; inherent clearances generate significant impact forces and peaks in the crank's actuating torque. The results demonstrate that flexible joints attenuate these torque peaks by nearly half. However, this flexibility introduces vibrations, which affect the mechanism's overall performance. This study compares mechanisms with flexible imperfect joints against those with perfect and imperfect rigid joints. Although flexible imperfect joints reduce torque peaks by approximately 50%, they introduce low-amplitude vibrations due to elasticity. Furthermore, simulations show that joint flexibility redistributes contact forces, decreasing the severity of impact stresses that typically accelerate wear and fatigue. These findings indicate that incorporating controlled flexibility into imperfect joints can substantially enhance operational smoothness and durability. Overall, this study provides critical insights for designing more reliable mechanical systems, particularly where joint clearances are unavoidable.

Keywords: Imperfect Joints, Flexible Joint, MBS, FEA.

1. Introduction

The performance of multibody mechanical systems (MBS) with imperfect joints has garnered considerable attention over the last two decades, driven by advancements in computational technology. A multibody mechanical system comprises links connected by joints. These systems can range from relatively simple configurations, such as a slider-crank linkage, to more complex assemblies, like the tracks of bulldozers, which typically consist of over fifty links connected by revolute joints. Crank-slider mechanisms, commonly used in internal combustion engines. Joints are considered perfect if there is no clearance between the journal's outer surface and the bearing's inner surface. However, in real-world applications, such clearances usually exist due to wear, rendering the joints imperfect. Perfect joints impose kinematic constraints on the system, whereas imperfect joints impose force-based constraints. To mitigate the effects of wear and extend the mechanism's lifespan, bushes made of softer materials are inserted into the joints to circulate lubricant, resulting in what is termed a flexible joint, as shown in Figure 1.

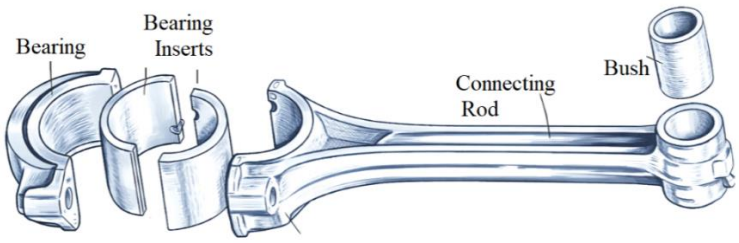

Figure 1. Bush and Bearing Inserts

* Corresponding author e-mail: bjalshaer@just.edu.jo.

Extensive research has addressed both lubricated [1–4] and dry [5–41] imperfect joints using analytical, numerical, and experimental approaches. Gummer and Sauer [5] used RecurDyn to simulate a slider-crank with imperfect joints. Abdallah et al. [6] and Zhao et al. [7] analyzed crank-slider and compressor mechanisms with flexible components and joint imperfections using MSC ADAMS. Luo et al. [8] validated a dry friction model in multibody systems via ADAMS. Tian et al. [9] used RecurDyn to model lubricated joints with journal misalignment. Zheng et al. [10] used co-simulation tools for flexible mechanisms with lubricated joints. Mukras et al. [11] studied wear in planar joints with oscillatory contacts using ANSYS. Su et al. [12] modeled flexible bushings with virtual massless links in ANSYS. Imed et al. [13], Sun and Xu [14], and Cammarata [15] investigated various clearance joint behaviors using AdamsTM. Other studies [16–26] confirm that flexible links generally reduce impact forces and stresses in imperfect joints. Omar [27] created a spatial algebra-based multibody framework for flexible bodies, using modal coordinates and inertia invariants for efficient dynamics, in [41], he extends this work with an energy-damping stabilization method to solve for static equilibrium in large systems, ensuring stable dynamic simulation starts. Both works minimize equations via connectivity matrices for computational efficiency.

Flores & Lankarani [28] developed a spatial multibody model for rigid mechanisms with lubricated spherical joints, combining a Hertzian contact law with Reynolds' squeeze-film theory to demonstrate that a fluid film significantly reduces impact forces. In [29], they extended this rigid-body approach to planar mechanisms with multiple clearance joints, showing how the number and size of clearances systematically alter the dynamic response. Costa et al. [30] applied similar joint models to human gait, finding that a lubricated joint model produces smoother force profiles than a dry-contact model, better matching physiological motion. Tian et al. [31] comprehensively surveyed methods for joints with clearance, comparing dry and lubricated models and highlighting open challenges. Marques et al. [32] analyzed closed-loop mechanisms, showing how an "elastic joint" formulation introduces virtual compliance. Flores et al. [33] reviewed continuous contact laws for frictional impacts, while [34] specifically integrated hydrodynamic lubrication into revolute joints to capture fluid-induced damping. Flores & Lankarani [35] further emphasized that compliance in multibody models typically originates from contact laws, not joint elasticity. Rodrigues da Silva et al. [36] compiled and assessed various Hertz-type compliant contact laws for impact simulation. Marques et al. [37, 40] reviewed friction modeling, underscoring its critical role in joint dynamics, and [38] proposed a novel LuGre-based model for complex transient effects. Finally, Marques et al. [39] analyzed spatial spherical-clearance joints with dry friction, quantifying how friction and clearance size affect a mechanism's response. Collectively, these works establish a framework where rigid-body models are augmented with sophisticated interface laws for contact, friction, and lubrication to simulate joint dynamics.

However, the inherent compliance provided by flexible bushings in imperfect joints - a pragmatic feature of real mechanisms - has been largely overlooked in prior studies. While several works have addressed related aspects, none have explicitly considered the compliance of joint bushings within imperfect (clearance) joints. Even recent comparative studies and state-of-the-art reviews emphasize the need for more comprehensive joint models to capture such effects. In contrast, our work directly integrates bushing flexibility into the joint model for both perfect and imperfect joints, enabling a clear evaluation of how joint compliance mitigates clearance-induced impacts. This approach - examining flexible-perfect and flexible-imperfect joints side-by-side with traditional rigid joints - provides a more realistic and complete understanding of system behavior

2. Dynamics of Multibody Systems with Flexible Clearance Joints

Indirect Various approaches have been utilized in the literature to model the dynamics of multibody mechanical systems that include both rigid and flexible bodies. One approach uses continuous models to obtain analytical solutions; however, this method results in an infinite number of degrees of freedom, limiting its application to simple, regular geometries like beams. Another approach is the Rayleigh-Ritz method, which uses modes to discretize the geometries, but it is still difficult to apply to complex shapes. A third approach is the Finite Element Method (FEM), which can handle complex geometries by discretizing the problem using various shape elements. FEM introduces elasticity to flexible bodies by dividing them into several sub-bodies (elements) interconnected by springs and dampers. The incremental finite element approach uses a shape function to describe small rotations and a convected coordinate system to describe finite rigid body motion. However, this approach involves a linearization of the equations of motion, which can lead to inaccurate inertia and zero strain in rigid bodies. In contrast, the Floating Frame of Reference Formulation (FFRF), which is extensively employed in flexible multibody simulations, results in a highly nonlinear inertia matrix. This matrix is characterized by significant inertia coupling between the reference motion and the elastic deformation and can be represented through a distinct set of inertia shape integrals dependent on the assumed displacement field. Shabana and Schwertassek [25] have demonstrated that the FFRF yields the same dynamic relationship as that obtained using large deformation finite element formulations. Therefore, this research utilizes the FFRF to derive the mathematical model describing the equations of motion. FFRF is an FEM-based approach that describes the motion of bodies in a multibody system through rigid and elastic coordinates attached to the bodies. This approach avoids motion linearization by using an intermediate element coordinate system.

2.1. Floating Frame of Reference Formulation

Figure 2 illustrates the configuration of planar flexible body *i*, which serves as a link within a multibody mechanical system. Two sets of coordinates are required to describe the position vector $\boldsymbol{q}_i$ of an arbitrary point (node) on body *i*: the rigid-body coordinates ($\boldsymbol{q}_i^r$) expressed in the inertial frame, and the flexible (elastic) coordinates ($\boldsymbol{q}_i^f$) expressed in the floating frame. Referring to Figure 2, the generalized coordinate vector is written as

$$\boldsymbol{q}_i = \begin{bmatrix} \boldsymbol{r}_i^o \\ \theta_i \\ \boldsymbol{q}_i^f \end{bmatrix} \quad (1)$$

where $\boldsymbol{r}_i^o$ and θ_i denote the position and orientation, respectively, of the body-fixed origin O_i. Points *P* and *P′* in Figure 2 correspond to the undeformed and deformed positions of a generic material point. From the geometry in Figure 2, the position of the deformed point *P′* is given by

$$\boldsymbol{r}_i^{P'} = \boldsymbol{r}_i^o + \boldsymbol{A}_i\boldsymbol{u}_i = \boldsymbol{r}_i^o + \boldsymbol{A}_i\left(\boldsymbol{u}_i^o + \boldsymbol{u}_i^f\right) \quad (2)$$

where $\boldsymbol{A}_i$ is the orthogonal rotation matrix transforming vectors from the floating frame to the inertial frame, $\boldsymbol{u}_i$ is the undeformed position of the point in the body frame, and $\boldsymbol{u}_i^f$ is the elastic deformation vector. Introducing the shape matrix $\boldsymbol{S}_i$, Equation (2) becomes

$$\boldsymbol{r}_i^{P'} = \boldsymbol{r}_i^o + \boldsymbol{A}_i\left(\boldsymbol{u}_i^o + \boldsymbol{S}_i\,\boldsymbol{q}_i^f\right) \quad (3)$$

The velocity of point P' is obtained by differentiating Equation (3):

$$\dot{\boldsymbol{r}}_i^{P'} = \dot{\boldsymbol{r}}_i^o + \dot{\boldsymbol{A}}_i\left(\boldsymbol{u}_i^o + \boldsymbol{S}_i\,\boldsymbol{q}_i^f\right) + \boldsymbol{A}_i\boldsymbol{S}_i\dot{\boldsymbol{q}}_i^f = \dot{\boldsymbol{r}}_i^o + \tilde{\boldsymbol{u}}_i^T\boldsymbol{\omega}_i + \boldsymbol{A}_i\boldsymbol{S}_i\dot{\boldsymbol{q}}_i^f \quad (4)$$

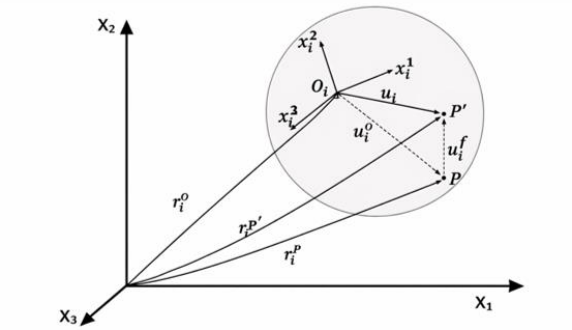

Figure 2. Flexible Body *i* Pose

where the overdot denotes time differentiation, ω_i is the angular velocity of body *i*, and $\tilde{\boldsymbol{u}}_i$ is the skew-symmetric matrix associated with $\boldsymbol{u}_i$. A second differentiation yields the acceleration:

$$\ddot{\boldsymbol{r}}_i^{P'} = \ddot{\boldsymbol{r}}_i^o + \boldsymbol{\omega}_i \text{ x } (\boldsymbol{\omega}_i \text{x} \boldsymbol{u}_i) + (\boldsymbol{\alpha}_i \text{x} \boldsymbol{u}_i) + 2\,\boldsymbol{\omega}_i \text{ x } \left(\boldsymbol{A}_i\,\tilde{\dot{\boldsymbol{u}}}_i\right) \quad (5)$$

with α_i representing the angular acceleration.

The kinetic energy of body *i* is expressed as $\frac{1}{2}\int\left(\rho_i\dot{\boldsymbol{r}}_i{}^T\dot{\boldsymbol{r}}_i\right)dV_i$, where $\rho_i$and $V_i$denote the material density and volume. Using this definition, the mass matrix takes the symmetric block form

$$\boldsymbol{M}_i = \begin{bmatrix} \boldsymbol{M}_i^{rr} & \boldsymbol{M}_i^{r\theta} & \boldsymbol{M}_i^{rf} \\ \boldsymbol{M}_i^{r\theta} & \boldsymbol{M}_i^{\theta\theta} & \boldsymbol{M}_i^{\theta f} \\ \boldsymbol{M}_i^{rf} & \boldsymbol{M}_i^{\theta f} & \boldsymbol{M}_i^{ff} \end{bmatrix} \quad (6)$$

For planar motion, the matrix components are

$$\boldsymbol{M}_i^{r_o r_o} = \begin{bmatrix} m_i & 0 \\ 0 & m_i \end{bmatrix} \quad (7.a)$$

$$\boldsymbol{M}_i^{r_o\theta} = \frac{d\boldsymbol{A}_i}{d\theta}\left(\int_{V_i}\rho_i\,\boldsymbol{u}_i^o dV_i + \left(\int_{V_i}\rho_i\boldsymbol{S}_i\,dV_i\right)\boldsymbol{q}_i^f\right) \quad (7.b)$$

$$\boldsymbol{M}_i^{r_o f} = \boldsymbol{A}_i\int_{V_i}\rho_i\boldsymbol{S}_i\,dV_i \quad (7.c)$$

$$\boldsymbol{M}_i^{\theta\theta} = \int_{V_i}\rho_i\,\boldsymbol{u}_i^{oT}\,\boldsymbol{u}_i^o\,dV_i + 2\left(\int_{V_i}\rho_i\boldsymbol{u}_i^{oT}\boldsymbol{S}_i dV_i\right)\boldsymbol{q}_i^f + \int_{V_i}\rho_i\boldsymbol{S}_i^T\,\boldsymbol{S}_i dV_i \quad (7.d)$$

$$\boldsymbol{M}_i^{\theta f} = \int_{V_i}\rho_i\,\boldsymbol{u}_i^{oT}\tilde{I}S_i dV_i + \boldsymbol{q}_i^f\left(\int_{V_i}\rho_i\left(\boldsymbol{S}_i^{1T}\,\boldsymbol{S}_i^2 - \boldsymbol{S}_i^{2T}\,\boldsymbol{S}_i^1\right)dV_i\right) \quad (7.e)$$

Here, $\boldsymbol{S}_i^1$ and $\boldsymbol{S}_i^2$denote the rows of the shape matrix $\boldsymbol{S}_i$ .For a linear isotropic material, the strain–displacement relation is

$$\boldsymbol{\varepsilon}_i = \boldsymbol{D}_i\,\boldsymbol{u}_i^f = \boldsymbol{D}_i\boldsymbol{S}_i\boldsymbol{q}_i^f \quad (8)$$

where $\boldsymbol{D}_i$ is the differential operator relating strains to displacements. The stress–strain relation is

$$\boldsymbol{\sigma}_i = \boldsymbol{E}_i\,\boldsymbol{\varepsilon}_i = \boldsymbol{E}_i\boldsymbol{D}_i\boldsymbol{S}_i\boldsymbol{q}_i^f \quad (9)$$

with $\boldsymbol{E}_i$ the symmetric elastic-constant matrix.The stiffness matrix associated with the elastic coordinates is

$$\boldsymbol{K}_i^{ff} = \int_{V_i}(\boldsymbol{D}_i\boldsymbol{S}_i)^T\boldsymbol{E}_i\boldsymbol{D}_i\boldsymbol{S}_i dV_i \quad (10.a)$$

The corresponding elastic force is

$$\boldsymbol{Q}_i^e = \begin{bmatrix} 0 & 0 & 0 \\ 0 & 0 & 0 \\ 0 & 0 & \boldsymbol{K}_i^{ff} \end{bmatrix}\boldsymbol{q}_i \quad (10.b)$$

As expected, rigid-body motion does not contribute to the potential energy, which depends solely on elastic deformation. The damping force vector is

$$\boldsymbol{Q}_i^d = \begin{bmatrix} 0 & 0 & 0 \\ 0 & 0 & 0 \\ 0 & 0 & \boldsymbol{C}_i^{ff} \end{bmatrix}\dot{\boldsymbol{q}}_i \quad (11)$$

where $\boldsymbol{C}_i^{ff}$ is the structural damping matrix.The total kinetic energy of the flexible body becomes

$$T = \frac{1}{2}\dot{\boldsymbol{q}}^T\boldsymbol{M}_i\dot{\boldsymbol{q}} \quad (12)$$

Lagrange's equation for body *i* in a multibody system is

$$\frac{d}{dt}\left(\frac{\partial T}{\partial\dot{\boldsymbol{q}}_i}\right)^T - \left(\frac{\partial T}{\partial\boldsymbol{q}_i}\right)^T + \boldsymbol{C}_{\boldsymbol{q}^T}^T\boldsymbol{\lambda} = \boldsymbol{Q}_i \quad (13)$$

where$\boldsymbol{C}_{\boldsymbol{q}^T}^T$ is the constraint Jacobian and **λ**is the vector of Lagrange multipliers.

Substituting the kinetic energy, virtual work contributions, and constraint relations yields

$$\boldsymbol{M}_i\ddot{\boldsymbol{q}}_i + \boldsymbol{K}_i\boldsymbol{q}_i + \boldsymbol{C}_{\boldsymbol{q}^T}^T\boldsymbol{\lambda} = \boldsymbol{Q}_i^e + \boldsymbol{Q}_i^v \quad (14)$$

where $\boldsymbol{Q}_i^v$ contains centrifugal and Coriolis forces, and $\boldsymbol{Q}_i^e$ includes applied forces such as gravity, springs, dampers, and actuators.In partitioned form, using the linear elastodynamic formulation:

$$\begin{bmatrix} \boldsymbol{M}_i^{rr} & \boldsymbol{M}_i^{rf} \\ \boldsymbol{M}_i^{rf} & \boldsymbol{M}_i^{ff} \end{bmatrix}\begin{bmatrix} \boldsymbol{q}_r^i \\ \boldsymbol{q}_f^i \end{bmatrix} = \begin{bmatrix} \overline{\boldsymbol{Q}}_i^r \\ \overline{\boldsymbol{Q}}_i^f \end{bmatrix} \quad (15)$$

For a complete multibody system with both rigid and flexible bodies, a more general system formulation is

$$\begin{bmatrix} \boldsymbol{M} & \boldsymbol{\Phi}_q^T & \boldsymbol{M}^{rm} \\ \boldsymbol{\Phi}_q & \boldsymbol{0} & -\boldsymbol{H} \\ (\boldsymbol{M}^{rm})^T & -\boldsymbol{H}^T & \boldsymbol{M}^{mm} \end{bmatrix}\begin{bmatrix} \ddot{\boldsymbol{q}} \\ -\boldsymbol{\lambda} \\ \ddot{\boldsymbol{q}}_{em} \end{bmatrix} = \begin{bmatrix} \mathbf{g} \\ \boldsymbol{\gamma} \\ \boldsymbol{Q} \end{bmatrix} \quad (16)$$

where $\boldsymbol{M}$ is the global Cartesian inertia matrix, $\boldsymbol{M}^{rm}$contains coupling terms between modal and reference accelerations, $\boldsymbol{M}^{mm}$is the modal inertia matrix, $\boldsymbol{\Phi_q}$ is the kinematic constraint Jacobian, $\boldsymbol{H}$is the joint influence matrix, and $\boldsymbol{Q}$ contains the joint force contributions. A detailed derivation of Equation (16) can be found in reference [27].

The flexible components used in this study, although implemented through a commercial multibody–finite-element co-simulation platform, are modeled according to the Floating Frame of Reference Formulation (FFRF) described earlier. In common multibody environments such as ADAMS, RecurDyn, and ANSYS–MBD interfaces, flexible bodies originate from a finite-element mesh and are subsequently reduced—either modally or nodally—to express their deformation relative to a body-attached floating reference frame. This procedure ensures that each component's motion is represented by a rigid reference trajectory with superimposed elastic coordinates, consistent with the theoretical framework outlined.

During numerical integration, the elastic coordinates are used to assemble the global mass, stiffness, and damping matrices and to enforce the associated kinematic constraints, in accordance with the formulations presented in Equations (14) – (16). Although the analysis interface appears graphical from the user's standpoint, the underlying solver executes the same computational procedures defined by the FFRF: it couples the reference and elastic coordinates, evaluates modal or element-level shape functions, and applies constraints directly to the deformable bodies. Consequently, the simulation environment does not approximate the theoretical formulation—it implements it

explicitly. This ensures that the predicted dynamic response of the flexible bush, as well as its interaction with the crank–slider mechanism, adheres closely to the mathematical model developed earlier and remains consistent with the assumptions applied throughout the methodology and results.

2.2. Viscoelastic Constitutive Model

The viscoelastic behavior of the deformable body is represented using a linear, isotropic Kelvin–Voigt material model, which is fully compatible with both the finite-element description and the Floating Frame of Reference Formulation (FFRF) summarized in Section 2.1. This constitutive framework decomposes the material response into an instantaneous elastic contribution and a viscosity-driven rate component, thereby preserving the small-strain assumption applied to the elastic deformation field of the flexible body.

Consistent with the strain–displacement relation defined in Eq. (8), the strain vector for body *i* is expressed as

$$\boldsymbol{\varepsilon}_i = \boldsymbol{B}_i \boldsymbol{q}_i^f \quad (17)$$

Where $\boldsymbol{B}_i$ is the space-dependent strain–displacement matrix, obtained from the differential operator D_i and the shape matrix $\boldsymbol{S}_i$, and $\boldsymbol{q}_i^f$ is the vector of elastic generalized coordinates introduced in Eq. (1).The elastic component of the stress follows the linear isotropic relation defined earlier in Eq. (9):

$$\sigma_i^e = \boldsymbol{C}_{e,i}\boldsymbol{\varepsilon}_i \quad (18)$$

where $\boldsymbol{C}_{e,i}$ is the symmetric elastic-constant matrix for body *i*. To account for internal damping, a viscous stress component proportional to the strain rate is added:

$$\boldsymbol{\sigma}_i^v = \boldsymbol{C}_{v,i}\dot{\varepsilon}_i \quad , \quad \dot{\varepsilon}_i = \boldsymbol{B}_i \dot{\boldsymbol{q}}_f \quad (19)$$

with $\boldsymbol{C}_{v,i}$ the viscous constitutive matrix. Thus, the total stress in the Kelvin–Voigt solid becomes

$$\boldsymbol{\sigma}_i = \boldsymbol{\sigma}_i^e + \boldsymbol{\sigma}_i^v = \boldsymbol{C}_{e,i}\boldsymbol{B}_i\boldsymbol{q}_i^f + \boldsymbol{C}_{v,i}\boldsymbol{B}_i\dot{\boldsymbol{q}}_i^f \quad (20)$$

Using this stress representation and the strain definition in Eq. (17), the internal virtual work of body iii can be written as

$$\delta W_{int,i} = \int \left(\boldsymbol{C}_{e,i}\boldsymbol{B}_i\boldsymbol{q}_i^f + \boldsymbol{C}_{v,i}\boldsymbol{B}_i\dot{\boldsymbol{q}}_i^f\right)\boldsymbol{B}_i\delta\boldsymbol{q}_i^f\, dV) \quad (21)$$

From Eq. (21), the internal elastic–viscous force vector associated with the flexible coordinates is obtained as

$$f_{int,i} = \boldsymbol{K}_i^{ff}\boldsymbol{q}_i^f + \boldsymbol{C}_i^{ff}\dot{\boldsymbol{q}}_i^f \quad (22)$$

where the elastic stiffness and structural damping matrices are

$$\boldsymbol{K}_i^{ff} = \int_V \boldsymbol{B}_i^T\boldsymbol{C}_{e,i}\boldsymbol{B}_i dV \;, \boldsymbol{C}_i^{ff} = \int_V \boldsymbol{B}_i^T\boldsymbol{C}_{v,i}\boldsymbol{B}_i dV \quad (23)$$

These matrices enter directly into the flexible-body equations of motion in Eq. (14) and integrate seamlessly with the elastic and damping contributions previously presented in Eqs. (10) and (11). Because the FFRF naturally accommodates large rigid-body motion combined with small elastic deformation, the Kelvin–Voigt constitutive model is fully compatible with the flexible multibody framework. Consequently, the viscoelastic terms influence both the internal elastic forces and the dissipative forces that appear in the global multibody dynamics of Eqs. (15) and (16), thereby ensuring a coherent and physically accurate representation of the flexible joint behavior.

3. Performance of a Crank–Slider Multibody System with a Dry Imperfect Flexible Joint: A Case Study

In this study, the dynamic performance of a crank–slider mechanism incorporating a dry imperfect flexible joint is evaluated. Figure 3and table 1 present the mechanism and identifies all relevant components and dimensions.

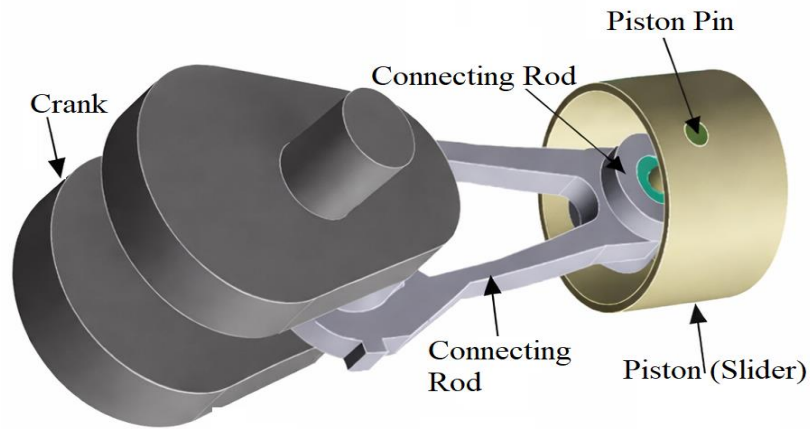

Figure 3. Crank–slider mechanism with the flexible joint under investigation

Table 1. Crank–slider mechanism imperfect joint specifications

Mass of the crank=1.30 kg	Inertia of the crank=5x10^{-2} kg.m^2	Length of the crank = 0.14 m	Mass of con. Rod = 3.37 kg	Inertia of con. Rod = 3.2x10^{-2} kg.m^2	Length of con. Rod = 0.32 m
Inner radius of bush=0.11 m	Outer radius of bush = 0.20 m	Piston pin radius=0.10 m	Length of the bush=0.032 m	Ang. Speed of crank=3000 rpm	Mass of slider=2.2 kg

The crank connects to the ground through an idealized revolute bearing with no clearance, whereas the slider–bush connection is modeled using a journal bearing (bushing), where clearance is commonly present in practice.

Although many prior studies represent this slider–bush interface as a perfect or rigid-imperfect joint, the present work models it explicitly as a flexible element to capture its compliance and influence on system dynamics. The investigation focuses on how introducing flexibility at the bushing affects internal joint forces and the reaction torque required to maintain a constant crank speed of 3000 rpm. Four joint configurations are examined: (i) Rigid-perfect joint: all joints rigid with zero clearance; (ii) Rigid-imperfect joint: slider–bush joint rigid but with clearance, following the classical model of Flores et al. [35] for comparison;(iii) Flexible-perfect joint: slider–bush joint flexible but without clearance;(iv) Flexible-imperfect joint: slider–bush joint flexible and including radial clearance. Clearance is introduced by increasing the bush's inner diameter such that the difference between the bush's inner radius and the journal's outer radius defines the clearance c. A perfect joint corresponds to c =0, whereas c >0 introduces an imperfect joint. The bush's outer surface is assumed to be rigidly attached to the connecting rod, enforcing zero displacement(u=0). When clearance exists, the journal contacts the inner surface of the bush, producing an indentation δ and corresponding boundary displacement (u=δ), as depicted in Figure 4.The flexible bushing is modeled in ANSYS using a plane-strain formulation, appropriate for long bushings where axial strains are negligible.

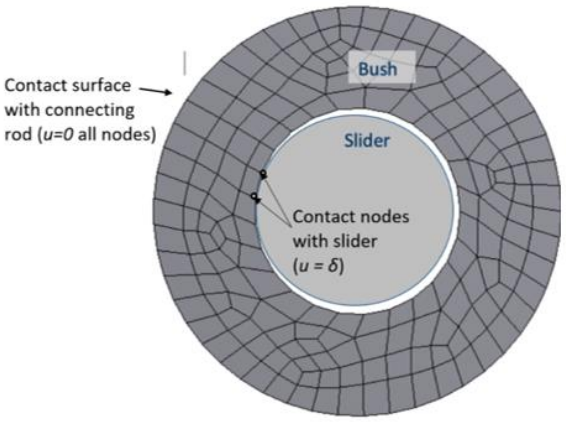

Figure 4. Meshing the bush and boundary conditions

The outer surface is constrained with fixed displacement to represent its rigid attachment, and the inner surface is defined either with zero clearance (perfect joint) or with a prescribed radial offset (imperfect joint). In the latter case, contact indentation is represented using a displacement constraint u=δ, enabling the model to capture the bushing's compliance without explicitly simulating impact phenomena. This approach is consistent with established practices in flexible multibody dynamics and finite-element contact modeling. The bushing material is assumed to be a typical tin–bronze alloy used in dry journal bearings, with elastic modulus E=110GPa, Poisson's ratioν=0.34, and density ρ=8800 kg/m^3. Material damping is represented through shear-viscosity η_s=300Pa·s and bulk-viscosity η_b = 900 Pa·s, capturing internal dissipation during localized deformation and approximating the alloy's viscoelastic energy loss.

The reaction torque, defined as the torque required to maintain the prescribed crank motion, is used as a key performance indicator because it reflects both inertial effects and the forces transmitted through the joint. Smoother and lower torque values correspond to more stable and efficient operation. In all numerical simulations, the crank speed is kept constant at 3000 rpm.

Figure 5 illustrates the motor torque required to maintain the imposed kinematic state (ω_{crank} = 3000 rpm), commonly referred to as motor sizing. Figure 5(a) presents the motor sizing results for a crank–slider mechanism with an ideal revolute joint. In this configuration, the absence of compliance or clearance leads to smooth internal reaction forces in both the y- and x-directions, as evidenced in Figure 6(a) and Figure 6(b), respectively, which in turn result in a smooth and steady torque profile, as shown in Figure 5(a). In Figure 5(b), joint flexibility is introduced, which induces high frequency variations in the internal reaction forces, as seen in Figure 6(c) and Figure 6(d). These fluctuations manifest as high-frequency oscillations in the motor torque, particularly pronounced at the start of motion. Figure 5(c) demonstrates the effect of introducing clearance into an otherwise ideal joint. The presence of clearance generates impact-type internal forces in both y and x directions, as illustrated in Figure 6(e) and Figure 6(f), leading to distinct sharp peaks in the motor torque shown in Figure 5(c).Finally Figure 5(d) shows the torque requirements when both flexibility and clearance are introduced into the joint, in this case; the y and x internal impact forces are attenuated by the existence of flexibility (as shown in figures 6(g) and Figure 6(h) respectively), this explains the attenuated peaks and the fluctuations in the motor sizing as Figure 5(d) demonstrates.

Figure 7 illustrates that introducing a flexibility imperfection at the slider–connecting rod joint leads to significantly elevated von Mises stress levels, marked by distinct spikes (dashed line), in contrast to the smoother stress profile of an ideal flexible joint (solid line). This highlights how minor imperfections in joint compliance can substantially intensify dynamic stress responses. Additionally, the finite element analysis in Figure 8for certain instant of time reveals concentrated stress zones at the revolute interface (red areas), further emphasizing the sensitivity of joint stress behavior to flexibility deviations.

Introducing flexibility fundamentally alters this response. Instead of a single sharp impulse as in rigid joints, the flexible bushing produces a distributed force response governed by its stiffness and damping. As a result, force peaks are reduced and followed by small damped oscillations due to the bushing's elastic recovery. Since rigid joints cannot store elastic energy, they do not exhibit comparable stress or force variations.

Figure 5 shows the torque required to maintain constant crank speed. Even with perfect rigid joints, the torque exhibits periodic fluctuations due to the slider's inherent reciprocating motion: acceleration peaks near the dead-center positions and decreases mid-stroke. These geometric effects dominate the baseline torque waveform. Superimposed on this are additional elastic contributions in the flexible-joint cases. As the radial force transmitted through the bush varies, the bushing deforms and recovers, introducing brief elastic transients twice per cycle. These transients generate higher-frequency oscillations superimposed on the fundamental kinematic torque pattern.

Clearance joints introduce further dynamics. Each contact event induces an elastic rebound in the flexible bush, and although Kelvin–Voigt damping dissipates this energy, the continuous reciprocating motion repeatedly excites the joint. This combination results in torque and force histories featuring both periodic kinematic variations and damped elastic vibrations.

A comparison of internal joint forces in Figure 6 reveals sharp contrast between rigid- and flexible-joint responses. In the rigid-imperfect model, an immediate high-amplitude impact occurs when the slider pin contacts the bush, producing an impulsive force spike. In the flexible-imperfect configuration, however, the initial peak is significantly lower because the bushing absorbs part of the impact energy. Following contact, the flexible joint exhibits decaying oscillations caused by cyclic loading and release of strain energy, whereas the rigid joint displays abrupt force transitions without post-impact dynamics. The results indicate that flexibility reduces peak joint forces by approximately 50%, though at the expense of small damped vibrations. Rigid-clearance joints transmit larger, sharper forces, while flexible joints smooth these interactions, extending the contact duration and lowering force magnitudes.

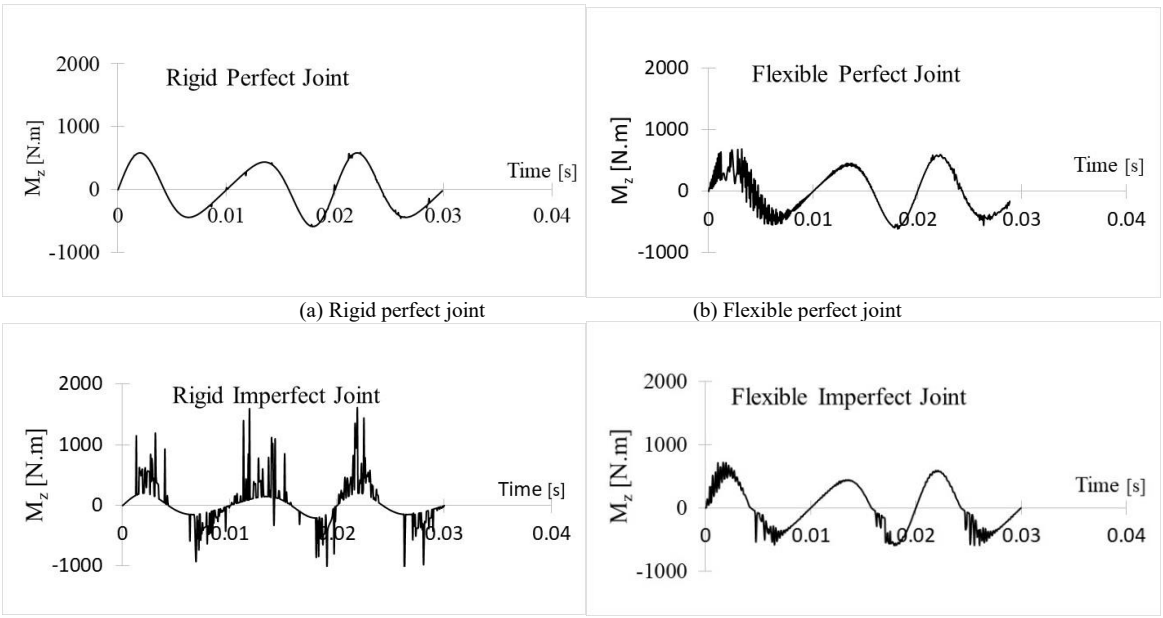

(a) Rigid perfect joint (b) Flexible perfect joint

(c) Rigid imperfect joint (d) Flexible imperfect joint

Figure 5. Motor sizing for the crank–slider mechanism

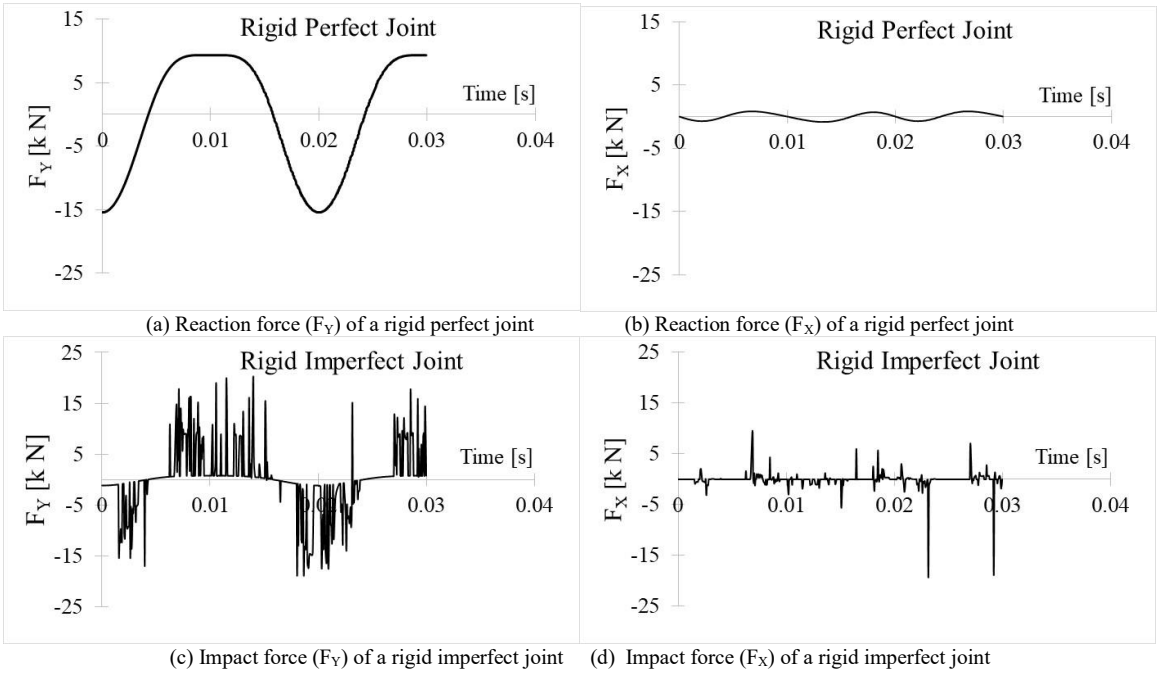

(a) Reaction force (F_Y) of a rigid perfect joint (b) Reaction force (F_X) of a rigid perfect joint

(c) Impact force (F_Y) of a rigid imperfect joint (d) Impact force (F_X) of a rigid imperfect joint

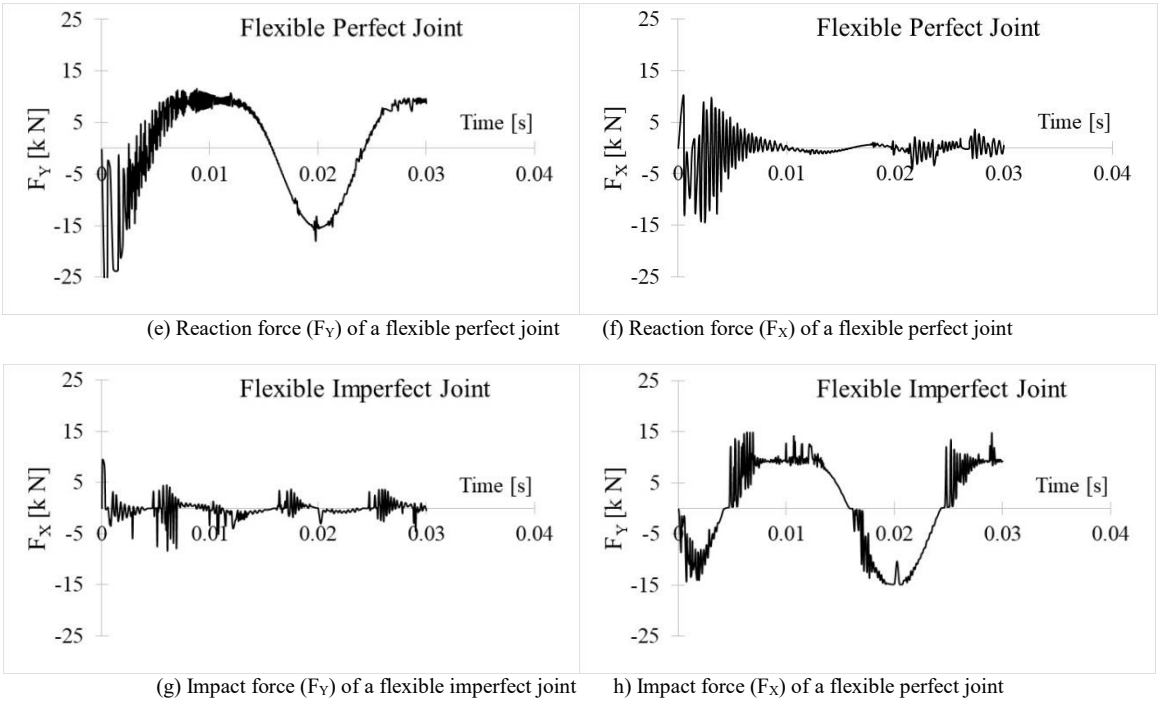

(e) Reaction force (F_Y) of a flexible perfect joint (f) Reaction force (F_X) of a flexible perfect joint

(g) Impact force (F_Y) of a flexible imperfect joint h) Impact force (F_X) of a flexible perfect joint

Figure 6. Joint internal forces in the crank–slider mechanism

Figure 7 shows that von Mises stress rises sharply at each contact event in clearance joints due to localized indentation. In perfect-joint models, where continuous contact is maintained, stresses remain low and smooth. In all flexible-joint cases, the maximum stresses occur along the contact interface, consistent with the regions of highest mechanical loading. Figure 8 further illustrates these spatial distributions, which help identify areas prone to yielding or fatigue under cyclic loading.

These observations align with prior studies. Flores et al. [35] reported similar high impact forces in rigid-clearance joints, while Tian et al. [9] and Abdallah et al. [6] found that flexibility in lubricated and dry joints substantially reduces peak forces and produces smoother signals with elastic oscillations due to material compliance. Gummer and Sauer [5] similarly showed that joint flexibility mitigates impact shocks and enhances force continuity. The present results extend these findings by showing that explicit modeling of the bushing's internal flexibility produces even greater reductions in peak forces without altering the mechanism's geometry.

Parametric studies on bushing stiffness and damping confirm these trends. A stiff bushing with clearance produces large impact spikes but minimal post-impact oscillation, behaving similarly to a rigid joint. A more compliant bushing softens the impact and reduces peak reaction torque by nearly 50% but introduces transient elastic oscillations, whose duration and amplitude depend on damping levels. Higher damping shortens these oscillations, while lower damping prolongs them.

From an engineering standpoint, these results emphasize the crucial role of tuning bushing stiffness and damping to achieve a desirable trade-off between shock absorption and vibration control. A sufficiently compliant, well-damped bushing can significantly reduce impact loads and torque spikes, enhancing durability and operational smoothness. However, excessive flexibility can introduce residual vibrations. Optimal joint performance requires selecting material and geometric properties that balance these competing effects.

The oscillatory behavior observed in both internal force and stress histories (Figures 6 and 7) is consistent with prior work on clearance joints [5, 6, 9]. The combination of clearance-induced impacts and bushing compliance ultimately governs the mechanism's dynamic response, confirming that flexibility within the joint can substantially reshape force transmission and stress distribution.

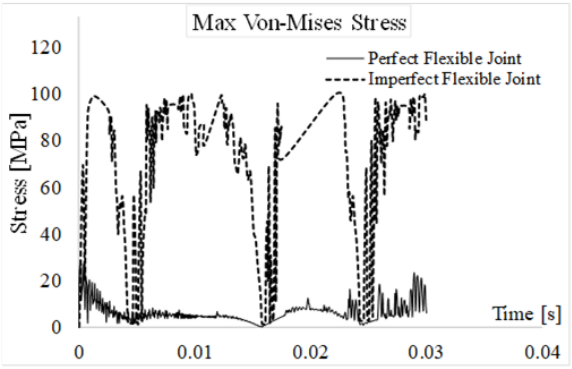

Figure 7. Flexible joint maximum stress.

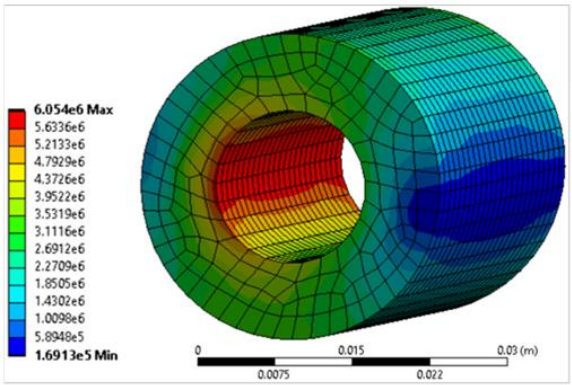

Figure 8. Temporal Typical Stress Distribution

4. Conclusions

Most previous studies on multibody systems with joint clearances have represented joints either as rigid-clearance connections or as idealized elastic couplings, without explicitly accounting for the realistic compliance of bushings. This omission is significant because local joint flexibility can strongly influence internal contact forces and required motor torque, directly affecting the performance and durability of high-speed mechanisms. In this work, a crank–slider mechanism operating at a constant speed of 3000 rpm was analyzed under four configurations: fully rigid, rigid with clearance, flexible without clearance, and flexible with clearance. The simulations show that incorporating joint compliance substantially softens impact loading. In particular, a flexible bush absorbs part of the collision energy and reduces peak reaction torque by nearly 50 % compared to the rigid-clearance case, while the internal contact forces increase more gradually and exhibit low-amplitude, damped oscillations instead of abrupt spikes. These results demonstrate that embedding local flexibility can significantly smooth dynamic load histories, albeit at the expense of mild elastic vibrations, revealing a clear trade-off between shock attenuation and vibration control.

The flexible bush behaves effectively as a spring–damper element within the joint. It cushions the impacts between the journal and the bearing, lowers peak contact forces and reaction torques, and then releases stored strain energy in the form of small, rapidly decaying oscillations. The viscous component of the Kelvin–Voigt material model ensures that these oscillations are quickly damped and do not persist throughout the motion. Overall, the flexible joint configuration replaces short-duration, high-magnitude impact shocks with smoother, lower-magnitude force and torque histories, consistent with the response of a damped elastic system.

Stress analysis further indicates that the maximum von Mises stresses are concentrated at the pin–bush contact interface. In joints with clearance, each collision produces a sharp local stress peak, whereas a zero-clearance joint exhibits a smoother and lower stress evolution until full contact is established. Introducing bushing compliance and damping distributes the load transfer over a longer time interval, thereby moderating the stress peaks even though the contact region remains the most severely stressed. These observations identify the critical locations susceptible to wear and fatigue and highlight the importance of selecting appropriate bushing materials, clearances, and geometries to control stress concentrations and extend service life under dynamic loading.

The present findings are consistent with previously reported trends for clearance joints and compliant elements. Earlier studies have shown that adding flexibility in links or joints reduces peak dynamic loads and smooths force histories. This work confirms that behavior and extends it by explicitly modeling compliance within the bushing itself. The results show that joint-embedded flexibility alone can achieve reductions in peak forces comparable to those obtained by modifying link flexibility, without altering the overall mechanism geometry. Thus, a significant portion of the shock-mitigating benefit can be realized by judicious choice of bushing properties.

From a design standpoint, the outcomes of this study emphasize the need to balance stiffness and damping in bushing design. Adequate compliance and internal damping can substantially mitigate impact forces and torque spikes, improve torque smoothness, and enhance component longevity, while avoiding unnecessary oversizing of the drive system. However, excessive compliance may introduce residual vibrations and degrade motion accuracy. An optimal bushing should therefore be soft enough to absorb shock loads, yet sufficiently stiff and well damped to preserve motion precision and minimize persistent oscillations. The quantitative results presented here provide guidance on how bushing flexibility influences forces, torques, and stresses in crank–slider mechanisms, and can assist engineers in selecting materials and clearances that enhance both durability and dynamic performance.

References

[1] Alshaer BJ, Lankarani HM. “An exact analytical solution for dynamic loads generated by lubricated long journal bearings”. *Mechanism and Machine Theory*. 2023; Vol. 183, 105263. https://doi.org/10.1016/j.mechmachtheory.2023.105263

[2] Alshaer BJ, Lankarani HM. “An exact analytical solution for dynamic loads generated by imperfect lubricated journal bearings in multibody systems”. *Multibody System Dynamics*. 2024. https://doi.org/10.1007/s11044-024-10020-6

[3] Alshaer BJ, Lankarani HM. “Multiple lubricated joints with long and short bearings in multibody mechanical systems - Modeling, simulation, and performance analysis”. *Mechanism and Machine Theory*. 2024; Vol. 203, 105815. https://doi.org/10.1016/j.mechmachtheory.2024.105815

[4] Flores P, Ambrósio J, Claro JCP, Lankarani HM, Koshy CS. “A study on dynamics of mechanical systems including joints with clearance and lubrication”. *Mechanism and Machine Theory*. 2005; Vol. 41, No. 3, pp. 247–261. https://doi.org/10.1016/j.mechmachtheory.2005.10.002

[5] Gummer A, Sauer B. “Modeling planar slider-crank mechanisms with clearance joints in RecurDyn”. *Multibody System Dynamics*. 2012; Vol. 31, pp. 127–145. https://doi.org/10.1007/s11044-012-9339-2

[6] Abdallah MAB, Khemili I, Aifaoui N. “Numerical investigation of a flexible slider–crank mechanism with multijoints with clearance”. *Multibody System Dynamics*. 2016; Vol. 38, No. 2, pp. 173–199. https://doi.org/10.1007/s11044-016-9526-7

[7] Zhao H, Xu M, Wang J, Chen G. “A dynamic analysis of reciprocating compressor transmission mechanism with joint clearance”. *Applied Mechanics and Materials*. 2012; Vols. 226–228, pp. 641–645. https://www.scientific.net/AMM.226-228.641

[8] Luo XM, Qi ZH, Kong XC. “Non-colliding contact analysis with friction in the planar prismatic joint”. *Chinese Journal of Computational Mechanics*. 2012; Vol. 29, No. 3, pp. 387–392. https://caod.oriprobe.com/articles/29834056/Non_colliding_contact_analysis_with_friction_in_th.htm

[9] Tian Q, Sun Y, Liu C, Hu HY, Flores P. “Elastohydrodynamic lubricated cylindrical joints for rigid–flexible multibody dynamics”. *Computers and Structures*. 2013; Vol. 114, pp. 106–120. https://doi.org/10.1016/j.compstruc.2012.10.019

[10] Zheng EL, Zhu R, Zhu SH, Lu XJ. “A study on dynamics of flexible multi-link mechanism including joints with clearance and lubrication for ultra-precision presses”. *Nonlinear Dynamics*. 2016; Vol. 83, No. 1, pp. 137–159. https://doi.org/10.1007/s11071-015-2315-7

[11] Mukras S, Kim NH, Sawyer WG, Jackson DB, Bergquist LW. “Numerical integration schemes and parallel computation for wear prediction using finite element method”. *Wear*. 2009; Vol. 266, pp. 822–832. https://doi.org/10.1016/j.wear.2008.12.016

[12] Su Y, Chen W, Tong Y, Xie Y. "Wear prediction of clearance joint by integrating multi-body kinematics with finite-element method". *Proceedings of the Institution of Mechanical Engineers, Part J: Journal of Engineering Tribology*. 2010; Vol. 224, No. 8, pp. 815–823. https://doi.org/10.1243/13506501JET783

[13] Imed K, Lotfi R. "Dynamic analysis of a flexible slider-crank mechanism with clearance". *European Journal of Mechanics - A/Solids*. 2008; Vol. 27, pp. 882–898. https://doi.org/10.1016/j.euromechsol.2007.12.004

[14] Sun J, Xu G. "Deviation analysis and optimization of offset slider-crank mechanism based on the simulation". *Information Technology Journal*. 2013; Vol. 12, No. 12, pp. 2390–2397. https://scialert.net/abstract/?doi=itj.2013.2390.2397

[15] Cammarata A. "A novel method to determine position and orientation errors in clearance-affected overconstrained mechanisms". *Mechanism and Machine Theory*. 2017; Vol. 118, pp. 247–264. https://www.sciencedirect.com/science/article/abs/pii/S0094114X17307449

[16] Dubowsky S, Moening MF. "An experimental and analytical study of impact forces in elastic mechanical systems with clearances". *Mechanism and Machine Theory*. 1978; Vol. 13, pp. 451–465. https://www.sciencedirect.com/science/article/abs/pii/0094114X78900186

[17] Tian Q, Zhang Y, Chen L, Flores P. "Dynamics of spatial flexible multibody systems with clearance and lubricated spherical joints". *Computers & Structures*. 2009; Vol. 87, pp. 913–929. https://doi.org/10.1016/j.compstruc.2009.03.006

[18] Erkaya S, Uzmay İ. "Effects of balancing and link flexibility on dynamics of a planar mechanism having joint clearance". *Scientia Iranica*. 2012; Vol. 19, No. 4, pp. 483–490. https://www.sciencedirect.com/science/article/pii/S1026309812000806

[19] LiY, Chen G, Sun D, Gao Y, Wang K. "Dynamic analysis and optimization design of a planar slider–crank mechanism with flexible components and two clearance joints". *Mechanism and Machine Theory*. 2016; Vol. 99, pp. 53–57.https://doi.org/10.1016/j.mechmachtheory.2015.11.018

[20] Ahmedalbashir M. *Dynamic analysis of flexible mechanisms with clearance*. Master's thesis. American University of Sharjah; 2016. https://repository.aus.edu/entities/publication/1bea71c0-681b-4c6f-9609-4183c0575f3e

[21] Alfrehat A. *Performance of Multibody Mechanical Systems with Imperfect Joints*. Master's thesis. Jordan University of Science and Technology; 2022.

[22] Pereira MFOS, Ambrósio JAC. *Computer-Aided Analysis of Rigid and Flexible Mechanical Systems*. Dordrecht: Kluwer Academic Publishers; 1994. https://link.springer.com/book/10.1007/978-94-011-1166-9

[23] Song JO, Haug EJ. "Dynamic analysis of planar flexible mechanisms". *Computer Methods in Applied Mechanics and Engineering*. 1980; Vol. 24, pp. 359–381. https://www.sciencedirect.com/science/article/abs/pii/0045782580900705

[24] Shabana AA. *Dynamics of Multibody Systems*. 5th ed. Cambridge: Cambridge University Press; 2020. https://www.cambridge.org/us/universitypress/subjects/engineering/solid-mechanics-and-materials/dynamics-multibody-systems?format=HB&isbn=9781108485647

[25] Shabana AA, Schwertassek R. "Equivalence of the floating frame of reference approach and finite element formulations". *International Journal of Non-Linear Mechanics*. 1998; Vol. 33, pp. 417–432.

[26] Simeon B. *Computational Flexible Multibody Dynamics: A Differential-Algebraic Approach*. Berlin: Springer; 2013. https://link.springer.com/book/10.1007/978-3-642-35158-7

[27] Omar M. "Modeling flexible bodies in multibody systems in joint-coordinates formulation using spatial algebra". *Advances in Mechanical Engineering*. 2014; Article ID 468986. https://doi.org/10.1155/2014/468986

[28] Flores P, Lankarani HM. "Spatial rigid multibody systems with lubricated spherical clearance joints: Modeling and simulation". *Nonlinear Dynamics*. 2010; Vol. 60, No. 1–2, pp. 99–114.

[29] Flores P, Lankarani HM. "Dynamic response of multibody systems with multiple clearance joints". *ASME Journal of Computational and Nonlinear Dynamics*. 2012; Vol. 7, No. 3, 031003. https://doi.org/10.1115/1.4005927

[30] Costa J, Peixoto J, Moreira P, Souto AP, Flores P, Lankarani HM. "Influence of hip joint modeling approaches on the kinematics of human gait". *Journal of Tribology*. 2016; Vol. 138, No. 3, 031201. https://doi.org/10.1115/1.4031988

[31] Tian Q, Flores P, Lankarani HM. "A comprehensive survey of the analytical, numerical, and experimental methodologies for dynamics of multibody mechanical systems with clearance or imperfect joints". *Mechanism and Machine Theory*. 2018; Vol. 122, pp. 1–57. https://doi.org/10.1016/j.mechmachtheory.2017.12.002

[32] Marques F, Roupa I, Silva MT, Flores P, Lankarani HM. "Examination and comparison of different methods to model closed-loop kinematic chains using Lagrangian formulation with cut joint, clearance joint constraint, and elastic joint approaches". *Mechanism and Machine Theory*. 2021; Vol. 160, 104294. https://doi.org/10.1016/j.mechmachtheory.2021.104294

[33] Flores P, Lankarani HM, Ambrósio J, Claro JCP. "Contact-impact events with friction in multibody dynamics: Back to basics". *Mechanism and Machine Theory*. 2023; Vol. 184, 105305. https://doi.org/10.1016/j.mechmachtheory. 2023. 105305

[34] Flores P, Lankarani HM. "Modelling lubricated revolute joints in multibody mechanical systems". *Proceedings of the Institution of Mechanical Engineers, Part K: Journal of Multi-body Dynamics*. 2004; Vol. 218, No. 4, pp. 183–190. https://doi.org/10.1243/1464419043541491

[35] Flores P, Lankarani HM. "State-of-the-art and challenges of contact-impact problems using multibody dynamics methodologies". In: Arczewski K, Blajer W, Fraczek J, Wojtyra M, editors. *Multibody Dynamics: Computational Methods and Applications*. Berlin: Springer; 2024, p. 233–241. https://doi.org/10.1007/978-3-031-67295-8_26

[36] Rodrigues da Silva M, Marques F, da Silva MT, Flores P. "A compendium of contact force models inspired by Hunt and Crossley's cornerstone work". *Mechanism and Machine Theory*. 2022; Vol. 167, 104501. https://doi.org/10.1016/j.mechmachtheory.2021.104501

[37] Marques F, Flores P, Claro JCP, Lankarani HM. "Modeling and analysis of friction including rolling effects in multibody dynamics: A review". *Multibody System Dynamics*. 2018; Vol. 45, pp. 223–244. https://doi.org/10.1007/s11044-018-09640-6

[38] Marques F, Woliński Ł, Wojtyra M, Flores P, Lankarani HM. "An investigation of a novel LuGre-based friction force model". *Mechanism and Machine Theory*. 2021; Vol. 166, 104493. https://doi.org/10.1016/j. mechmachtheory. 2021. 104493

[39] Marques F, Isaac F, Dourado N, Souto AP, Flores P, Lankarani HM. "A study on the dynamics of spatial mechanisms with frictional spherical clearance joints". *Journal of Computational and Nonlinear Dynamics*. 2017; Vol. 12, No. 5, 051013. https://doi.org/10.1115/1.4036480

[40] Marques F, Flores P, Lankarani HM. "On the frictional contacts in multibody system dynamics". In: Arczewski K, Blajer W, Fraczek J, Wojtyra M, editors. *Multibody Dynamics: Computational Methods and Applications*. Berlin: Springer; 2016, p. 67–91. https://doi.org/10.1007/978-3-319-30614-8_4

[41] Omar M. "Static Analysis of Large-Scale Multibody System Using Joint Coordinates and Spatial Algebra Operator". *The Scientific World Journal*. 2014; Article ID 409402. http://dx.doi.org/10.1155/2014/409402